JOURNAL OF THERMOPHYSICS AND HEAT TRANSFER
Vol. 33, No. 1, January–March 2019

Electron-Impact Ionization of Atomic Nitrogen

Christopher J. Ciccarino*
Harvard University, Cambridge, Massachusetts 02138
and
Daniel W. Savin†
Columbia University, New York, New York 10027

DOI: 10.2514/1.T5463

New electron-impact ionization (EII) data are presented for neutral atomic nitrogen. The atom is treated as a 67-state system, incorporating Rydberg values up to $n = 20$. State-specific cross sections for the first three states are from published *B*-spline *R*-matrix-with-pseudostates results. Binary-encounter Bethe calculations have been performed for the remaining 64 states. These data are designed for modeling the hypersonic chemistry that occurs when a space vehicle enters Earth's atmosphere from beyond orbit. The cross sections have been convolved into state-specific thermal rate coefficients and fit with the commonly used Arrhenius–Kooij formula for ease of use in shock-heated air plasma models. Additionally, rate coefficients are provided for a reduced 10-state system for use in coarse-grain models. For a given collisional–radiative model, these fine- and coarse-grain data can be used to generate state-specific rate coefficients for three-body electron–ion recombination, the time-reverse process of EII.

Nomenclature

a_0	=	Bohr radius (5.292×10^{-9} cm)
B	=	binding energy
B_i	=	binding energy of the target electron for state i
$\tilde{B}_j$	=	binding energy for grouped state j
E_i	=	excitation energy for state i
$\tilde{E}_j$	=	excitation energy for grouped state j
$E_{\max}$	=	maximum excitation energy included in a particular structure model
$f(T, \mathcal{T}_e)$	=	Maxwell–Boltzmann electron energy distribution
f_1	=	amplitude fitting parameter used in the Drawin equation
f_2	=	logarithm fitting parameter used in the Drawin equation
g_i	=	statistical weight for state i
i	=	state number
J	=	total angular momentum
j	=	grouped state number
k_B	=	Boltzmann constant (8.617×10^{-5} eV · K^{-1})
k_i	=	electron-impact ionization rate coefficient for state i
L	=	total orbital angular momentum
ℓ	=	orbital angular momentum quantum number
m_e	=	electron mass (511.0 keV/c^2)
N	=	occupation number of electrons in the target $n\ell$ orbital
n	=	principal quantum number
$n_{\max}$	=	maximum principal quantum number included in a particular structure model
p	=	linear momentum
R	=	Rydberg energy (13.61 eV)
S	=	total spin angular momentum
$\lvert s \rvert$	=	reduced dipole length
T	=	collision energy
$\mathcal{T}_e$	=	electron temperature
$T_{\max}$	=	maximum integration energy for the Maxwell–Boltzmann electron energy distribution
t	=	reduced collision energy (T/B)
$t_{\max}$	=	reduced maximum integration energy ($T_{\max}/B$)
U	=	average orbital kinetic energy ($\langle p^2/2m_e \rangle$)
U_i	=	average orbital kinetic energy of the target electron for state i
u	=	reduced average orbital kinetic energy (U/B)
v_e	=	electron collision velocity
α_i	=	Arrhenius–Kooij formula preexponential factor for state i
β_i	=	Arrhenius–Kooij formula temperature power for state i
γ_i	=	Arrhenius–Kooij formula activation parameter for state i
σ_i	=	total electron-impact ionization cross section for state i
$\sigma_{\mathrm{DI},i}$	=	direct ionization cross section for state i
$\sigma_{\mathrm{EA},i}$	=	excitation-autoionization cross section for state i
$\sigma(n\ell)$	=	electron-impact ionization direct ionization cross section for an $n\ell$ electron

I. Introduction

SPACE vehicles returning to Earth from beyond orbit enter the atmosphere at hypersonic velocities (greater than Mach 5). The resulting shock front generates a high-temperature reactive plasma flowing past the vehicle (a flowfield with temperatures on the order of 10,000 K). This intense heat is transferred to the capsule by radiative and convective means. Modeling the processes that a vehicle undergoes as it passes through the atmosphere and designing spacecraft to withstand these conditions requires an accurate understanding of the underlying nonequilibrium high-temperature chemistry [1].

Especially important is the chemistry of nitrogen, which is the dominant element in Earth's atmosphere. Atomic N line emission can be a major source of radiative heating during atmospheric entry, particularly in the afterbody region of the vehicle (i.e., downstream from the leading edge or forebody) [2]. Vacuum ultaviolet (VUV) line emission, in the ∼100–200 nm bandpass, is predicted to contribute over 85% of the total heating of the afterbody [3].

Recent work by West et al. [2] indicates that this predicted heat flux is highly sensitive to the calculated number density of neutral atomic N. This number density depends, in part, on the reaction

Presented as Paper 2018-1716 at the AIAA SciTech 2018, Kissimmee, FL, 8–12 January 2018; received 27 January 2018; revision received 26 April 2018; accepted for publication 27 May 2018; published online 20 September 2018.

*Graduate Student, Department of Chemistry and Chemical Biology, 12 Oxford Street.

†Senior Research Scientist, Columbia Astrophysics Laboratory, 550 West 120th Street, MC 5247. Member AIAA.

$$N + e^- \underset{b}{\overset{f}{\rightleftharpoons}} N^+ + e^- + e^- \quad (1)$$

Electron-impact ionization (EII), the forward reaction (f), ionizes N atoms in the forebody region of the flowfield. In the afterbody region, N^+ undergoes the backward reaction (b), three-body electron–ion recombination (TBR). Reliable TBR data are among the data needed to accurately quantify the N number density in the afterbody region and the associated heating of the capsule. These TBR data are calculated from the corresponding EII data using detailed balance through the principle of microreversibility. Johnston and Brandis [3] find that the VUV heating of the afterbody is primarily due to TBR. Hence, uncertainties in the EII data affect the TBR data, the predicted N abundance, and thereby the predicted radiative heating of the afterbody.

In the work of West et al. [2], they use a global (i.e., effective) rate coefficient for EII of atomic N, implicitly approximating the gas as being in a quasi-steady state (QSS). This practice of assuming that a given species can be modeled using a single EII rate coefficient is often necessary to make hypersonic entry models more computationally tractable. West et al. assign an order of magnitude uncertainty to the N EII rate coefficient used. They also report that a $\mp 50\%$ change in the N EII rate coefficient can cause up to a $+125/-50\%$ change, respectively, in the radiative heat flux on the afterbody. These effects would likely be even more severe if the full order of magnitude uncertainty were included. Clearly, reliable N EII data are needed to accurately predict the radiative heat flux on the afterbody of an entry vehicle.

More sophisticated hypersonic chemical models of atomic N employ a collisional–radiative (CR) approach and treat the various electronic states of N as independent species [4–12]. However, this requires reliable EII data for a large number of states. The issue then arises of how to generate these data [13]. Laboratory measurements, at best, can provide unambiguous data only for the ground state [14,15]. Often they yield ambiguous results due to the presence of an unknown fraction of metastable states in the target [16]. Ultimately, theory must be relied on to generate the needed EII data, but many of the past approaches used are of questionable accuracy, as we discuss later.

Here, we present new EII calculations for neutral atomic N. The atom is treated as a 67-state system, incorporating Rydberg values up to $n = 20$. For use in coarse-grain simulations, we also present a reduced-model structure, which combines our 67 states into 10 groupings. We provide both sets of results in a format that can be readily integrated into chemical models. The rest of the paper is organized as follows. Section II briefly reviews past electronic structure models for atomic N and presents the model we use here. Section III highlights important aspects of the EII process, the state of the art for experimental and theoretical studies, and presents our new EII calculations. Section IV compares our cross-section results to those from earlier approaches used to generate N EII data. Section V reports our new thermal EII rate coefficients and the fits to the data. Last, Sec. VI summarizes our results.

II. Electronic Structure Model

Numerous structure models for atomic N have been presented in the literature for use in CR models of air plasmas formed during entry into Earth's atmosphere. Table 1 ([5–12,16–28]), gives a broad selection of the published models, listed by increasing number of states included. We have used these previously published results as a guide in developing our own structure model. In particular, we have built on the work of Park [5] and Panesi et al. [12], adding in missing states, and following the lead of Park [6] by extending the structure up to the $n = 20$ Rydberg state. Potapov et al. [7] also presented a model with nearly as many states as ours. Unfortunately, they do not adequately describe their structure model for us to use as a detailed guide.

In Table 2, we present our 67-state model for the structure of atomic N. For each state i, we give the configurations (and terms) included, the statistical weight g_i, the excitation energy E_i above the ground state ($i = 1$), the binding or ionization energy B_i, and the average orbital kinetic energy U_i. States are denoted by their configuration and, when specified, specific LS term(s). Here, L is the total orbital angular momentum, and S is the total spin angular momentum. States for which no terms are listed are assumed to comprise all possible LS terms for the given configurations. Note that we do not specify the total angular momentum J values, which are designated in spectroscopy as levels.

The required values of U_i were obtained using multiconfiguration Hartree–Fock calculations [32]. For the binding and excitation energies, we used the National Institute of Standards and Technology (NIST) database [29] where data were available. Those data are presented down to the J levels. Such a degree of detail is not necessary for our work. To represent B_i and E_i for an LS term, we statistically average over the J levels within the term. For the states in Table 2 that are composed of more than one term, we statistically average over the available LS term data to obtain the corresponding binding and excitation energies.

The NIST database did not include all data needed for our 67 states, and in general many high-lying states had limited experimental data available. We obtained values of B_i and E_i for state 40 by statistically averaging the data from Erikkson [30]. In a similar manner, for states 42, 48, 51, 54, and 56 we used data from de Beer et al. [31], which correspond to np terms for $n = 6$, 7, 8, 9, and 10, respectively. We also use their data for states 46 and 50, which are given for a limited set of terms in $\ell = 3$. We generalize these $\ell = 3$ data by assuming that they are well-representative of the binding and excitation energies of the composite state. A similar procedure was followed for states 53, 57, 58, and 59 using the limited NIST data, which include data only up to $\ell = 2$. For states $i > 59$, we extrapolate from the available NIST data for $n = 9$–12 by assuming that the highly excited atomic nitrogen system can be treated as hydrogenic, with $E_i \propto n_i^{-2}$.

For comparison to other works, we provide the state numbers from the models of Park [5] and Panesi et al. [12]. Our model includes more states than that of Park; we have separated terms that he grouped together and added the $n = 15$–20 states. Our model also has more states than that of Panesi et al. because we have included both $n \leq 9$ and $n = 10$–20 states that they did not include.

Table 1 Published EII models for atomic N, showing number of states i included, highest bound state energy E_{max}, highest Rydberg number n_{max}, and the EII source

				EII source		
Model	Number of states	E_{max}, eV	n_{max}	$i = 1$	$i = 2$–3	$i \geq 4$
Taylor and Ali [8]	13	12.36	3	Drawin [17]	Drawin [17]	Drawin [17]
Kunc and Soon [9]	14	12.92	4	Brook et al. [16]	Sobelman et al. [18]	Gryziński and Kunc [19]
Johnston [11]	35	14.412	10	Drawin [20]	Drawin [20]	Drawin [20]
Park (1973) [6]	35	14.499	20	Lotz [21]	Lotz [21]	Lotz [21]
Park (1968) [5]	41	14.463	14	Gryziński [22]	Gryziński [22]	Gryziński [22]
Bourdon and Vervisch [10]	43	14.463	14	Brook et al. [16]	Sobelman et al. [18]	Gryziński and Kunc [19]
Panesi et al. [12]	46	14.331	9	Tawara and Kato [23]	Kim and Desclaux [24]	Drawin [25]
Potapov et al. [7]	63	14.350	9	Thomson [26]	Thomson [26]	Thomson [26]
Present work	67	14.522	20	Wang et al. [27]	Wang et al. [27]	Hwang et al. [28]

Table 2 Atomic N electronic structure used (unmarked values of E_i and B_i from NIST)

State number i										
Present	Park [5]	Panesi et al. [12]	Configurations (and terms) included	g_i	E_i, eV	B_i, eV	U_i, eV	α_i, $\mathrm{cm^3 \cdot s^{-1} \cdot K^{-\beta_i}}$	β_i	γ_i, K
1	1	1	$2s^22p^3(^4\mathrm{S^o})$	4	0	14.534	51.053	5.688×10^{-12}	7.210×10^{-1}	1.679×10^{5}
2	2	2	$2s^22p^3(^2\mathrm{D^o})$	10	2.384	12.150	49.624	7.215×10^{-11}	5.487×10^{-1}	1.401×10^{5}
3	3	3	$2s^22p^3(^2\mathrm{P^o})$	6	3.576	10.958	48.684	1.625×10^{-11}	6.691×10^{-1}	1.266×10^{5}
4	4	4	$2s^22p^2(^3\mathrm{P})3s(^4\mathrm{P})$	12	10.332	4.202	5.976	9.332×10^{-10}	4.873×10^{-1}	4.912×10^{4}
5	5	5	$2s^22p^2(^3\mathrm{P})3s(^2\mathrm{P})$	6	10.687	3.847	3.437	1.667×10^{-9}	4.539×10^{-1}	4.509×10^{4}
6	6	6	$2s2p^4(^4\mathrm{P})$	12	10.927	3.607	49.943	6.570×10^{-11}	7.416×10^{-1}	4.166×10^{4}
7	7	7	$2s^22p^2(^3\mathrm{P})3p(^2\mathrm{S^o})$	2	11.603	2.931	3.783	3.736×10^{-9}	4.214×10^{-1}	3.458×10^{4}
8	8	8	$2s^22p^2(^3\mathrm{P})3p(^4\mathrm{D^o})$	20	11.758	2.776	3.318	4.819×10^{-9}	4.076×10^{-1}	3.282×10^{4}
9	9	9	$2s^22p^2(^3\mathrm{P})3p(^4\mathrm{P^o})$	12	11.842	2.692	3.042	5.603×10^{-9}	3.993×10^{-1}	3.187×10^{4}
10	10	10	$2s^22p^2(^3\mathrm{P})3p(^4\mathrm{S^o})$	4	11.996	2.538	2.067	8.295×10^{-9}	3.752×10^{-1}	3.013×10^{4}
11	10	11	$2s^22p^2(^3\mathrm{P})3p(^2\mathrm{D^o})$	10	12.006	2.528	1.996	8.537×10^{-9}	3.734×10^{-1}	3.002×10^{4}
12	11	12	$2s^22p^2(^3\mathrm{P})3p(^2\mathrm{P^o})$	6	12.125	2.409	1.801	1.052×10^{-8}	3.621×10^{-1}	2.867×10^{4}
13	12	13	$2s^22p^2(^1\mathrm{D})3s(^2\mathrm{D})$	10	12.357	2.177	4.862	7.705×10^{-9}	3.964×10^{-1}	2.595×10^{4}
14	13	14	$2s^22p^2(^3\mathrm{P})4s(^4\mathrm{P})$	12	12.857	1.677	2.111	4.472×10^{-8}	2.852×10^{-1}	2.035×10^{4}
15	13	15	$2s^22p^2(^3\mathrm{P})4s(^2\mathrm{P})$	6	12.919	1.615	1.539	5.873×10^{-8}	2.673×10^{-1}	1.966×10^{4}
16	14	16	$2s^22p^2(^3\mathrm{P})3d(^2\mathrm{P})$	6	12.972	1.562	1.643	4.927×10^{-8}	2.848×10^{-1}	1.904×10^{4}
17	14	17	$2s^22p^2(^3\mathrm{P})3d(^4\mathrm{F})$	28	12.984	1.550	1.642	5.060×10^{-8}	2.834×10^{-1}	1.890×10^{4}
18	14, 15	18	$2s^22p^2(^3\mathrm{P})3d(^4\mathrm{P}, ^2\mathrm{F})$	26	13.000	1.534	1.575	5.416×10^{-8}	2.791×10^{-1}	1.872×10^{4}
19	15	19	$2s^22p^2(^3\mathrm{P})3d(^4\mathrm{D})$	20	13.019	1.515	1.534	5.667×10^{-8}	2.767×10^{-1}	1.851×10^{4}
20	15	20	$2s^22p^2(^3\mathrm{P})3d(^2\mathrm{D})$	10	13.035	1.499	1.445	6.056×10^{-8}	2.725×10^{-1}	1.833×10^{4}
21	16	21	$2s^22p^2(^3\mathrm{P})4p(^2\mathrm{S^o})$	2	13.202	1.332	1.585	1.134×10^{-7}	2.341×10^{-1}	1.645×10^{4}
22	17	22	$2s^22p^2(^3\mathrm{P})4p(^4\mathrm{D^o})$	20	13.244	1.290	1.472	1.310×10^{-7}	2.257×10^{-1}	1.597×10^{4}
23	17	23	$2s^22p^2(^3\mathrm{P})4p(^4\mathrm{P})$	12	13.268	1.266	1.400	1.429×10^{-7}	2.206×10^{-1}	1.570×10^{4}
24	18	24	$2s^22p^2(^3\mathrm{P})4p(^2\mathrm{D^o})$	10	13.294	1.240	1.052	1.713×10^{-7}	2.079×10^{-1}	1.541×10^{4}
25	18	25	$2s^22p^2(^3\mathrm{P})4p(^4\mathrm{S^o})$	4	13.322	1.212	1.068	1.847×10^{-7}	2.042×10^{-1}	1.510×10^{4}
26	18	26	$2s^22p^2(^3\mathrm{P})4p(^2\mathrm{P^o})$	6	13.343	1.191	0.982	2.020×10^{-7}	1.987×10^{-1}	1.486×10^{4}
27	19	27	$2s^22p^2(^3\mathrm{P})5s(^4\mathrm{P})$	12	13.624	0.910	1.086	5.764×10^{-7}	1.402×10^{-1}	1.168×10^{4}
28	19	28	$2s^22p^2(^3\mathrm{P})5s(^2\mathrm{P})$	6	13.648	0.886	0.864	6.799×10^{-7}	1.293×10^{-1}	1.140×10^{4}
29	20, 21	29	$2s^22p^2(^3\mathrm{P})4d$	90	13.679	0.855	0.883	6.578×10^{-7}	1.357×10^{-1}	1.105×10^{4}
30	21	30	$2s^22p^2(^3\mathrm{P})4f$	126	13.693	0.841	0.851	7.050×10^{-7}	1.317×10^{-1}	1.089×10^{4}
31	19, 22	31	$2s^22p^2(^1\mathrm{D})3p(^2\mathrm{D}, ^2\mathrm{F})$	24	13.718	0.816	2.786	1.262×10^{-7}	2.741×10^{-1}	1.054×10^{4}
32	23	32	$2s^22p^2(^3\mathrm{P})5p(^2\mathrm{S^o})$	2	13.770	0.764	0.879	1.114×10^{-6}	1.037×10^{-1}	1.002×10^{4}
33	23, 24	33	$2s^22p^2(^3\mathrm{P})5p(^4\mathrm{D^o}, ^2\mathrm{P^o}, ^4\mathrm{P^o})$	38	13.792	0.742	0.789	1.248×10^{-6}	9.717×10^{-2}	9.767×10^{3}
34	24	34	$2s^22p^2(^3\mathrm{P})5p(^4\mathrm{S^o})$	4	13.824	0.710	0.651	1.559×10^{-6}	8.316×10^{-2}	9.400×10^{3}
35	24	35	$2s^22p^2(^3\mathrm{P})5p(^2\mathrm{D^o})$	10	13.872	0.662	0.646	1.957×10^{-6}	7.136×10^{-2}	8.853×10^{3}
36	25	36	$2s^22p^2(^1\mathrm{D})3p(^2\mathrm{P^o})$	6	13.925	0.609	2.097	8.120×10^{-7}	1.526×10^{-1}	8.267×10^{3}
37	26	37	$2s^22p^2(^3\mathrm{P})6s(^4\mathrm{P}, ^2\mathrm{P})$	18	13.969	0.565	0.624	3.711×10^{-6}	3.400×10^{-2}	7.735×10^{3}
38	27	38	$2s^22p^2(^3\mathrm{P})5d$	90	13.992	0.542	0.563	3.867×10^{-6}	3.481×10^{-2}	7.478×10^{3}
39	27	39	$2s^22p^2(^3\mathrm{P})5f$	126	14.000	0.534	0.544	4.085×10^{-6}	3.165×10^{-2}	7.385×10^{3}
40	27	— —	$2s^22p^2(^3\mathrm{P})5g$	162	14.006[a]	0.528[a]	0.544	4.237×10^{-6}	2.980×10^{-2}	7.317×10^{3}
41	28	40	$2s^22p^2(^3\mathrm{P})6p(^4\mathrm{D^o}, ^4\mathrm{P^o})$	32	14.055	0.479	0.530	6.277×10^{-6}	6.674×10^{-3}	6.744×10^{3}
42	28	— —	$2s^22p^2(^3\mathrm{P})6p(^4\mathrm{S^o}, ^2\mathrm{D^o}, ^2\mathrm{P^o}, ^2\mathrm{S^o})$	22	14.084[b]	0.450[b]	0.443	8.005×10^{-6}	-7.470×10^{-3}	6.403×10^{3}
43	29	41	$2s^22p^2(^3\mathrm{P})7s$	18	14.150	0.384	0.420	1.364×10^{-5}	-3.639×10^{-2}	5.627×10^{3}
44	29	42	$2s^22p^2(^3\mathrm{P})6d$	90	14.162	0.372	0.390	1.438×10^{-5}	-3.763×10^{-2}	5.492×10^{3}
45	29	43	$2s^22p^2(^3\mathrm{P})6f$	126	14.167	0.367	0.378	1.505×10^{-5}	-4.010×10^{-2}	5.433×10^{3}
46	29	— —	$2s^22p^2(^3\mathrm{P})6\ell(\ell = 4\text{–}5)$	594	14.172[c]	0.362[c]	0.378	1.567×10^{-5}	-4.212×10^{-2}	5.374×10^{3}
47	30	44	$2s^22p^2(^3\mathrm{P})7p(^4\mathrm{D^o})$	20	14.201	0.333	0.373	2.109×10^{-5}	-5.883×10^{-2}	5.023×10^{3}
48	30	— —	$2s^22p^2(^3\mathrm{P})7p(^4\mathrm{P^o}, ^4\mathrm{S^o}, ^2\mathrm{D^o}, ^2\mathrm{P^o}, ^2\mathrm{S^o})$	34	14.215[b]	0.319[b]	0.334	2.462×10^{-5}	-6.762×10^{-2}	4.852×10^{3}
49	31	45	$2s^22p^2(^3\mathrm{P})8s + 7d$	108	14.263	0.271	0.288	3.921×10^{-5}	-9.069×10^{-2}	4.276×10^{3}
50	31	— —	$2s^22p^2(^3\mathrm{P})7\ell(\ell = 3\text{–}6)$	720	14.272[c]	0.262[c]	0.278	4.317×10^{-5}	-9.547×10^{-2}	4.167×10^{3}
51	32	— —	$2s^22p^2(^3\mathrm{P})8p$	54	14.298[b]	0.236[b]	0.252	5.988×10^{-5}	-1.128×10^{-1}	3.840×10^{3}
52	33	46	$2s^22p^2(^3\mathrm{P})9s$	18	14.322	0.212	0.230	8.216×10^{-5}	-1.290×10^{-1}	3.536×10^{3}
53	33	— —	$2s^22p^2(^3\mathrm{P})8\ell(\ell = 2\text{–}7)$	1080	14.336[d]	0.198[d]	0.213	9.646×10^{-5}	-1.359×10^{-1}	3.366×10^{3}
54	34	— —	$2s^22p^2(^3\mathrm{P})9p$	54	14.354[b]	0.180[b]	0.195	1.266×10^{-4}	-1.495×10^{-1}	3.131×10^{3}
55	35	— —	$2s^22p^2(^3\mathrm{P})10s + 9\ell(\ell = 2\text{–}8)$	1404	14.381[d]	0.153[d]	0.168	1.910×10^{-4}	-1.685×10^{-1}	2.782×10^{3}
56	36	— —	$2s^22p^2(^3\mathrm{P})10p$	54	14.393[b]	0.141[b]	0.156	2.113×10^{-4}	-1.738×10^{-1}	2.709×10^{3}
57	37	— —	$2s^22p^2(^3\mathrm{P})10\ell(\ell = 2\text{–}9)$	1728	14.414[d]	0.120[d]	0.136	3.474×10^{-4}	-1.956×10^{-1}	2.335×10^{3}
58	38	— —	$2s^22p^2(^3\mathrm{P})11\ell(\ell = 0\text{–}10)$	2178	14.437[d]	0.097[d]	0.112	5.693×10^{-4}	-2.168×10^{-1}	2.010×10^{3}
59	39	— —	$2s^22p^2(^3\mathrm{P})12\ell(\ell = 0\text{–}11)$	2592	14.460[d]	0.074[d]	0.097	1.021×10^{-3}	-2.403×10^{-1}	1.671×10^{3}
60	40	— —	$2s^22p^2(^3\mathrm{P})13\ell(\ell = 0\text{–}12)$	3042	14.473[e]	0.061[e]	0.081	1.520×10^{-3}	-2.555×10^{-1}	1.468×10^{3}
61	41	— —	$2s^22p^2(^3\mathrm{P})14\ell(\ell = 0\text{–}13)$	3528	14.484[e]	0.050[e]	0.071	2.247×10^{-3}	-2.696×10^{-1}	1.288×10^{3}
62	— —	— —	$2s^22p^2(^3\mathrm{P})15\ell(\ell = 0\text{–}14)$	4050	14.494[e]	0.040[e]	0.062	3.410×10^{-3}	-2.837×10^{-1}	1.116×10^{3}
63	— —	— —	$2s^22p^2(^3\mathrm{P})16\ell(\ell = 0\text{–}15)$	4608	14.502[e]	0.032[e]	0.055	5.082×10^{-3}	-2.963×10^{-1}	9.706×10^{2}
64	— —	— —	$2s^22p^2(^3\mathrm{P})17\ell(\ell = 0\text{–}16)$	5202	14.509[e]	0.025[e]	0.048	7.914×10^{-3}	-3.118×10^{-1}	9.036×10^{2}
65	— —	— —	$2s^22p^2(^3\mathrm{P})18\ell(\ell = 0\text{–}17)$	5832	14.514[e]	0.020[e]	0.043	1.165×10^{-2}	-3.216×10^{-1}	7.776×10^{2}
66	— —	— —	$2s^22p^2(^3\mathrm{P})19\ell(\ell = 0\text{–}18)$	6498	14.518[e]	0.016[e]	0.039	1.704×10^{-2}	-3.339×10^{-1}	7.109×10^{2}
67	— —	— —	$2s^22p^2(^3\mathrm{P})20\ell(\ell = 0\text{–}19)$	7200	14.522[e]	0.012[e]	0.035	2.474×10^{-2}	-3.379×10^{-1}	5.435×10^{2}
N^+	— —	— —	$2s^22p^2(^3\mathrm{P})$	— —	14.534	0	— —	— —	— —	— —

[a]Eriksson [30].
[b]de Beer (weighted) [31].
[c]de Beer (limited) [31].
[d]NIST (limited) [29].
[e]Extrapolated from NIST data [29].

Table 3 State groupings j for our coarse-grain model, including grouped excitation ($\tilde{E}_j$) and binding ($\tilde{B}_j$) energies and fitting parameters ($\alpha_j, \beta_j, \gamma_j$) for use in Eq. (11)

j	i included	$\tilde{E}_j$, eV	$\tilde{B}_j$, eV	α_j, $\mathrm{cm^3 \cdot s^{-1} \cdot K^{-\beta_i}}$	β_j	γ_j, K
1	1	0.000	14.534	5.688×10^{-12}	7.210×10^{-1}	1.679×10^{5}
2	2	2.384	12.150	7.215×10^{-11}	5.487×10^{-1}	1.401×10^{5}
3	3	3.576	10.958	1.625×10^{-11}	6.691×10^{-1}	1.266×10^{5}
4	4–6	10.641	3.893	2.360×10^{-9}	4.116×10^{-1}	4.845×10^{4}
5	7–13	11.951	2.583	1.958×10^{-8}	2.925×10^{-1}	3.253×10^{4}
6	14–21	12.985	1.549	6.453×10^{-8}	2.620×10^{-1}	1.916×10^{4}
7	22–27	13.342	1.192	3.215×10^{-7}	1.585×10^{-1}	1.558×10^{4}
8	28–52	14.121	0.413	1.604×10^{-4}	-2.522×10^{-1}	8.922×10^{3}
9	53–59	14.418	0.116	5.401×10^{-4}	-2.193×10^{-1}	2.255×10^{3}
10	60–67	14.506	0.028	1.101×10^{-2}	-3.230×10^{-1}	8.372×10^{2}

Using a high-fidelity representation of the electronic structure, however, increases the computational requirements for modeling hypersonic flows. To make such multidimensional simulations more tractable, one can bin the electronic states into a reduced number of groupings, thereby generating a "coarse-grain" or "reduced-order" structure model. This enables one to move away from the questionable QSS assumption of using a global rate coefficient to model nonequilibrium chemical processes. But it does raise the question of the accuracy of these coarse-grain models.

Panesi and Lani [33] reduced the 46-state N structure of Panesi et al. [12] into eight groupings. The first three correspond to the ground electronic state ($i = 1$) and the two metastable states ($i = 2$–3). The next five represent groupings of their remaining 43 states. Using a simulated chemical reactor, they found that the coarse-grain structure in general reproduced well the results obtained using the higher-fidelity original structure. They also found reasonable agreement with measurements from the well-known FIRE II flight experiment. The reduced model adequately matched the nonequilibrium phenomena observed during the early part of the reentry trajectory when nonequilibrium effects are expected to be most important.

A similar approach was taken by Lopez et al. [34], but they also investigated the accuracy of the reduced-order model as a function of the number of groupings. They found that the number of groupings could be reduced to seven while still maintaining an acceptable accuracy for the resulting EII and TBR rate coefficients. We use these results as a guide in constructing our reduced-order model.

Here, we present a coarse-grain model that follows the logic and procedure laid out in Panesi and Lani [33]. It is equivalent to their model for the first seven groupings. The eighth grouped state is also nearly identical, except that we have included several $n \leq 9$ states not given in Panesi et al. [12]. To this eight-grouping model, we have added two additional groupings to account for the $n = 10$–20 states.

Table 3 presents our reduced-order model. The state groupings are denoted by the index j and the states included by the index i, defined in Table 2. The grouped excitation energy $\tilde{E}_j$ and grouped ionization energy $\tilde{B}_j$ have been calculated following the equations of Panesi and Lani [33]. Not given here are the internal partition functions of each state grouping j, which can be calculated using the method presented in their work.

III. Cross-Section Data

A. Background

EII of atomic N is due to the sum of direct ionization (DI) and excitation–autoionization (EA) [24,27,35]. The EII cross section σ_i can be written for state i as

$$\sigma_i = \sigma_{\mathrm{DI},i} + \sigma_{\mathrm{EA},i} \tag{2}$$

where $\sigma_{\mathrm{DI},i}$ is the cross section for DI, and $\sigma_{\mathrm{EA},i}$ is that for EA. The direct process is represented as the forward direction of reaction 1. The EA process can be expressed as

$$\mathrm{N} + \mathrm{e^-} \rightarrow \mathrm{N^{**}} + \mathrm{e^-} \rightarrow \mathrm{N^+} + \mathrm{e^-} + \mathrm{e^-} \tag{3}$$

where $\mathrm{N^{**}}$ represents an excited state of N embedded in the $\mathrm{N^+}$ continuum. This intermediate state can either autoionize to form $\mathrm{N^+}$ or radiatively relax back to a bound state of N. In a system as light as N, autoionization dominates over fluorescence [36]. However, EA of atomic N turns out to be significant only for the two metastable states, as we briefly now discuss.

For the three terms in the $2s^2 2p^3$ ground configuration ($i = 1$–3), Wang et al. [27] have found that EA proceeds primarily via the strong $2s \rightarrow 2p$ one-electron transition, with an excitation energy of ~13.1 eV [35]. Because this energy is below the ionization threshold of the ground state, only the two metastable terms with their lower binding energies can undergo EA (see also [24]). But Wang et al. found that EA contributes only weakly to the EII process for these terms. Moving to higher excitations that start from the ground configuration, EA via a $2 \rightarrow n'$ transition ($n' \geq 3$) can be expected to be even less important [35]. To understand why, we remind the reader that autoionization is due to an electron–electron repulsion. The overlap of the excited electron with the core electrons rapidly decreases with increasing principal quantum number n', and the autoionization rate falls off roughly as $(n')^{-3}$ [37].

Also of little importance is EA starting from higher excited states such as the $2s^2 2p^2 n\ell$ configurations, where ℓ is the orbital angular momentum quantum number. Here, the excitation can proceed via $2p \rightarrow n'\ell'$ and $2s \rightarrow 2p$ or $n'\ell'$ ($n' \geq 3$). The largest of these EA channels are predicted to be via $2s \rightarrow 2p$ transitions, with an excitation energy of ~12.2 eV. But Abdel-Naby et al. [35] showed that DI dominates over EA for $n = 3$. The contribution of EA can be expected to be even smaller for higher n because the DI cross section grows roughly with the binding energy as B^{-2} (i.e., as n^4) [24], whereas autoionization decreases rapidly with increasing n' as described previously.

B. Relevant Collision Energies

Our goal here is to provide state-specific thermal EII rate coefficients for hypersonic chemical models. The corresponding electron temperature range spans $\mathcal{T}_e \sim 5000$–30,000 K ($k_B \mathcal{T}_e \sim$ 0.43–2.59 eV). Hence, state-specific cross-section data are needed for electron translational energies T from the ionization threshold B to $T_{\max} \approx B + 6k_B\mathcal{T}_e$, where k_B is the Boltzmann constant. This range comprises over 99% of the above-threshold portion of the Maxwell–Boltzmann (MB) electron energy distribution (EED) contributing to the state-specific thermal rate coefficients [38]. We can reexpress this cutoff in units of the reduced collision energy $t = T/B$, giving $t_{\max} \approx 1 + 6k_B\mathcal{T}_e/B$. The value of $t_{\max}$ increases roughly as n^2. Thus, for $n = 2$, the near-threshold behavior of the cross section is most important, but as n increases, so does the relevant t range needed to generate reliable EII rate coefficients.

C. State of the Art

EII of atomic N for the valence shell has been measured by Brook et al. [16]. Their results are shown in Fig. 1 as a function of the collision energy T. Unfortunately, the ion beam in that work contained an unknown fraction of metastable atoms, limiting the usefulness of the results for chemical modeling.

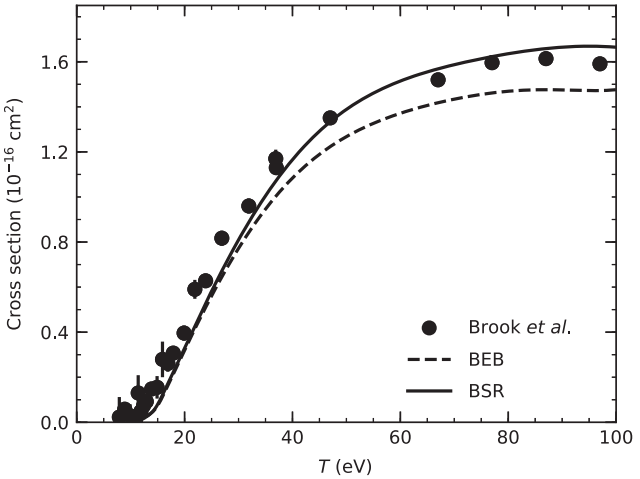

Fig. 1 EII cross-section data showing experimental (Brook et al. [16]) and theoretical (BEB [24], BSR [27]) results. See text for details.

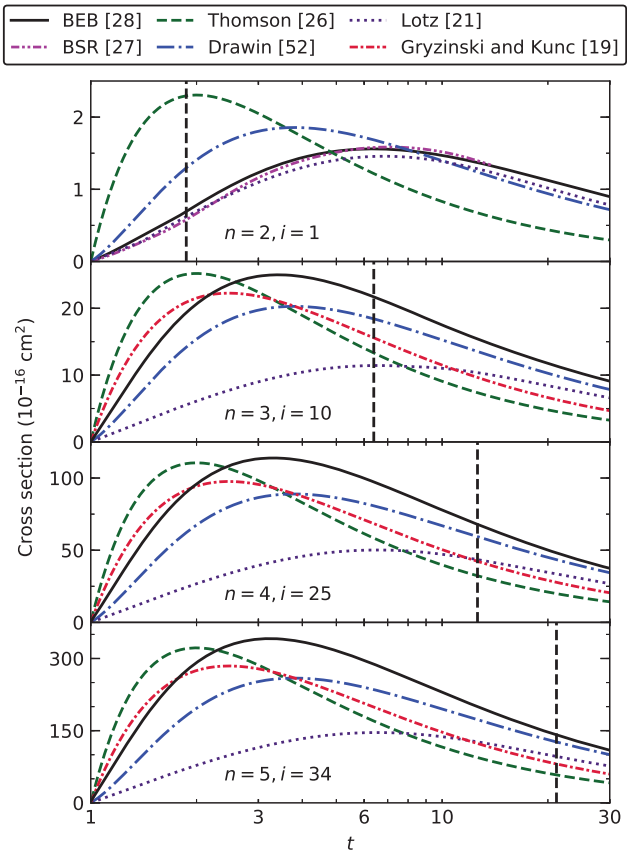

Fig. 2 Various theoretical EII cross sections for states $i = 1$, 10, 25, and 34.

For higher-lying electronic states, data from EII experiments are unlikely any time in the near future. This is due to the challenge of producing a sufficient target population in excited states because they can undergo rapid radiative dipole transitions to lower-lying states. Hence, theory must be relied on to generate the bulk, if not all, of the EII data needed for modeling air plasmas.

The state of the art for quantum mechanical EII calculations of atomic N are those of Wang et al. [27]. Their ab initio work was performed using the *B*-spline *R*-matrix-with-pseudostates (BSR) method. To compare these calculations to the experimental results, we have first convolved the theory with the experimental energy spread. Then, scaling the convolved theory for the ground and metastable terms and fitting to the data of Brook et al. [16] using a least-squares fitting weighted by the experimental uncertainties, we find good agreement with the experimental results for a beam of ∼85% ground term ^{4}S^o and ∼15% for the combined ^{2}D^o and ^{2}P^o metastable terms. The two metastable terms are so close together in magnitude and energy dependence that it is not possible to fit for them individually. The scaled BSR results are shown in Fig. 1. The BSR method can be used for states 1–3. However, the limits of current computational capabilities mean that the BSR approach is not yet tractable for calculating EII of higher-lying states.

A more computationally tractable quantum approach for DI is the binary-encounter dipole (BED) method of Kim and Rudd [39]. This approach starts with the Mott theory for the collision of two free electrons, using binary encounter theory to account for the momentum distribution of the bound electron, and combines it with the leading dipole part of the Bethe theory. The method is free of adjustable or fitted parameters. For ionization out of a given $n\ell$ subshell, it requires only the orbital occupation number, binding energy, average kinetic energy, and differential dipole oscillator strength. The orbital binding energies and average kinetic energies are relatively easy to either measure or calculate.

More challenging theoretically and experimentally are obtaining the necessary differential dipole oscillator strengths, particularly subshell by subshell. To overcome this issue, Kim and Rudd [39] introduced a simple form for the differential oscillator strength, which they called the binary-encounter Bethe (BEB) model. Like the BED method, the BEB approach is free of adjustable or fitted parameters. The BEB method has been extensively tested against laboratory studies and found to reproduce well the measured energy dependence and typically to agree to within ∼10% at the peak in the cross section [40].

In an attempt to more accurately calculate the differential oscillator strength, Huo [41] represented it using a convergent series, in what she called the improved binary-encounter dipole (iBED) method. She also presented a truncated version of the series for a simplified version of the iBED model. However, the complexity of the equations given for both methods makes them difficult to use with confidence. Fortunately, Huo found that the BEB and iBED methods have very similar energy dependences and agree to within ∼10% at the cross-section peak. This seems to us to be an acceptable level of agreement for hypersonic chemical models; thus, we favor here the computationally simpler BEB approach.

This BEB method was applied by Kim and Desclaux [24] to EII of atomic N, with scaled plane-wave Born cross sections used to account for EA of the metastable states. Figure 1 compares their theoretical results to the experimental work of Brook et al. [16] and the calculations of Wang et al. [27]. We have convolved the Kim and Desclaux results [24] with the experimental energy spread and scaled the ground and metastable terms using the beam fractions determined previously. Good agreement can be seen between the two sets of theoretical results. This can also be seen in Figs. 2 and 3, which shows the BEB and BSR cross sections and their ratio for the ground term, for which EA is not possible. In each figure, the dashed vertical lines show $t_{\max}$ for $\mathcal{T}_e = 30{,}000$ K. Figure 3 shows that the two methods agree within ∼20% at threshold, with improved agreement at higher collision energies. Note that a log (ratio) of ±0.3 corresponds to greater than a factor of 2 difference. This is promising because the BEB method, though less sophisticated than the BSR method, has been extended to DI of higher shells [28,42–44].

More recently, Huo [45] used the iBED method to calculate the atomic N EII cross sections for states $i = 1$–5 and 7–11. Lopez et al. [34] plan to incorporate her results into their future work. Once her data become publicly available, it will be good to compare our calculations here with hers, as a check of the relative accuracy of the two methods.

D. Present Electron-Impact Ionization Model

Based on the good agreement between the experimental data of Brook et al. [16] and the quantum BSR [27] and BEB [24] calculations, as well as between the iBED and BEB approaches [41], we have chosen to use a combination of the BSR and BEB methods to develop a new EII model for atomic N. For states 1–3, we used the published BSR data of Wang et al. [27]. We use the BEB method to

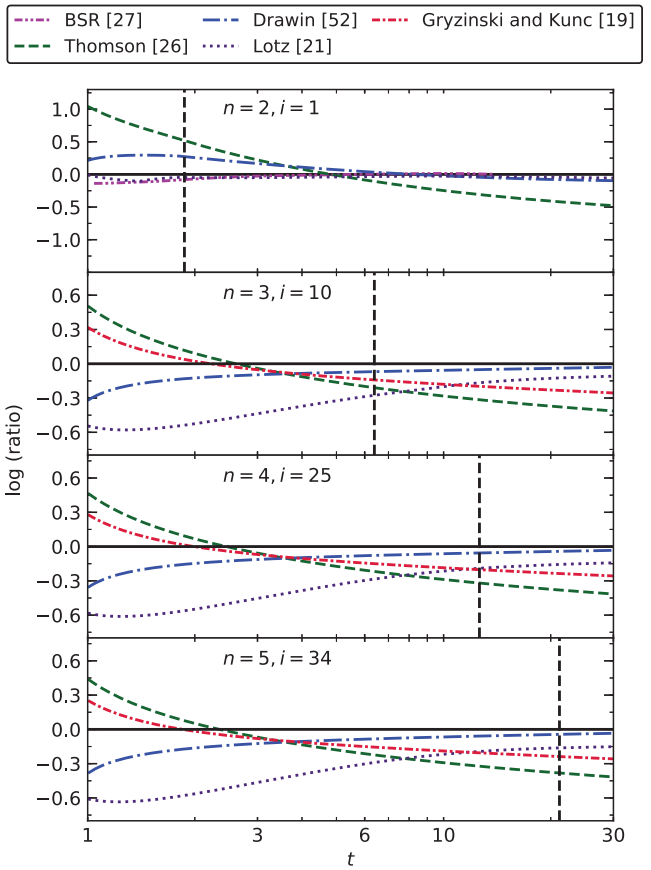

Fig. 3 Same as Fig. 2 but for the ratio of the EII cross section from other methods to that of the BEB. See text for details.

generate the DI data for the remaining states 4–67, keeping in mind that EA is expected to be unimportant for these states. Additionally, we only consider ionization into the $2s^2 2p^2(^3\mathrm{P})$ ground term of N^+. The ionization–excitation process forming an excited state of N^+ is predicted to be negligibly small [27].

The BEB DI cross section for an $n\ell$ electron in the K or L shell for a given state in Table 1 can be expressed as [39]

$$\sigma(n\ell) = \frac{4\pi a_0^2 N (R/B)^2}{t+u+1}\left[\frac{\ln t}{2}\left(1-\frac{1}{t^2}\right)+1-\frac{1}{t}-\frac{\ln t}{1+t}\right] \quad n \le 2 \tag{4}$$

Here, a_0 is the Bohr radius, N is the orbital occupation number of electrons, and R is the Rydberg energy. The quantity u is the reduced average orbital kinetic energy U/B, where $U = \langle p^2/2m_e \rangle$ is the average orbital kinetic energy for an electron with linear momentum p and mass m_e. On the right-hand side of Eq. (4), the terms N, B, t, and u are all state-dependent functions of $n\ell$.

In the BEB cross section [28,39,42–44], the $t+u+1$ denominator of the prefactor on the right-hand side arises from binary encounter theory, which sets the effective collision energy equal to the incident translational energy T plus the potential energy of the bound electron $|U+B|$. At large values of t, the prefactor behaves as $1/t$, as predicted by the Born approximation.

Moving to the term in square brackets, the first term, $(\ln t/2)(1–1/t^2)$, describes large impact parameter collisions. These are dominated by the dipole interaction and are given here by the leading dipole part of the Bethe theory. The remaining terms are from the Mott cross section, which describes a collision between two unbound electrons. Mott's theory does not take into account the dipole interaction because this only arises for bound electrons [46]. However, the Mott cross section is effective at describing small impact parameter collisions, where the dipole interaction is less important. The $1–1/t$ portion represents the direct and pure exchange terms of the Mott cross section, whereas the $\ln t/(1+t)$ represents the interference between the two.

For DI out of the M shell, or higher Rydberg states, good agreement between the BEB method and experimental results has been found by scaling the BEB cross section as [28,42–44,46]

$$\sigma(n\ell) = \frac{4\pi a_0^2 N (R/B)^2}{t+(u+1)/n}\left[\frac{\ln t}{2}\left(1-\frac{1}{t^2}\right)+1-\frac{1}{t}-\frac{\ln t}{1+t}\right] \quad n \ge 3 \tag{5}$$

Theoretical justification for the $1/n$ scaling has been given by Huo and Kim [43] and Ali et al. [47]. For high Rydberg states, the excited electron is loosely bound to the nucleus, and the DI cross section should approach that for a free–free collision. This is described by the Mott cross section, which varies simply as $1/t$. By introducing the $(u+1)/n$ scaling, the prefactor goes to $1/t$ as n increases.

The total BEB DI cross section for a given state i is then a summation over all $n\ell$ electrons in the target:

$$\sigma_i = \sum_{n\ell \in i} \sigma(n\ell) \tag{6}$$

However, for states 4–67, we really only need to consider DI of the outermost electron. Ionization of an inner-shell electron is unimportant under hypersonic conditions because the EED lies almost entirely below the ionization thresholds for these inner-shell electrons. As a result, readers wishing to generate BEB cross sections for states 4–67 can directly use the appropriate BEB equation [Eq. (4) or Eq. (5)] for the outermost occupied orbital and omit the summation over the $n\ell$ orbitals given in Eq. (6). The B and U values for the outermost electron are given in Table 2. For completeness, we also give the values for $i = 1$–3, but we stress that, for these states, we use the BSR cross-section calculations of Wang et al. [27].

IV. Comparison to Previous Electron-Impact Ionization Data

A number of approaches have been used over the years to generate the state-specific EII data needed for modeling shock-heated air plasmas. In this section, we review these other methods, compare them to the BSR and BEB results, and discuss their shortcomings.

Potapov et al. [7] used the classical EII cross section of Thomson [26] as given in [48]. The Thomson cross section can be expressed as

$$\sigma(n\ell) = \frac{4\pi a_0^2 N (R/B)^2}{t}\left[1-\frac{1}{t}\right] \tag{7}$$

Compared to experimental results, the Thomson cross section does a poor job of reproducing the measured data [49–51]. At low energies, it overestimates the cross section. There are two main reasons for this. First, the Thomson cross section assumes that the bound electron is stationary, and so it lacks the binary encounter correction in the denominator of the prefactor for the effective collision energy. Second, although the Thomson theory includes a term similar to the direct and pure exchange term of the Mott theory, it does not include a term for the interference between the two. This interference plays an important role in reducing the theoretical cross section near threshold. At higher energies, the Thomson theory underestimates the EII cross section because it does not account for the dipole interaction. Figures 2 and 3 compare the Thomson cross section to the BSR and BEB theory and demonstrate that this classical theory is systematically off, independent of n.

Gryziński has also developed several different classical theories for EII. Park [5] used the results of Gryziński [22], but these were later improved upon by Gryziński and Kunc [19]. Here, we compare only to these newer results, which were used for states $i \ge 4$ by Kunc and Soon [9] and Bourdon and Vervisch [10]. The classical cross section of Gryziński and Kunc can be expressed as

$$\sigma(n\ell) = \frac{4\pi a_0^2 N (R/B)^2}{[(t+1)^{1/2}+1]^2}\left[1 - \frac{1}{t} + \frac{2}{(t+1)^{1/2}}\left(1 - \frac{1}{t}\right) + \frac{2}{3}\left(1 - \frac{1}{t^2}\right)\right] \tag{8}$$

Because this formula was used for excited states, where typically only one electron occupied the highest orbital and $U \approx B$ (see e.g., Table 2), we have made the approximation of setting $U = B$ in our reexpression of their equation. We have also expressed the formula in a form that allows for easy comparison with the BEB method. Compared to available BSR and BEB data, Figs. 2 and 3 show that this classical theory still overestimates the EII cross section at low energies and underestimates it at high energies, but in each case less so than the Thomson theory. The denominator in the prefactor helps to reduce the cross section near threshold because Gryziński and Kunc developed their cross section using binary encounter theory. However, the term in the square brackets works in the opposite direction at low t, leading to the overestimate near the threshold. In part, this is because the interference term between the direct and exchange terms is missing. At higher energies, the theory does not include the dipole interaction, given by the Bethe theory. Thus, rather than asymptotically going to $\ln t/t$, the Gryziński and Kunc theory goes to $5/(3t)$. As shown in Figs. 2 and 3, this leads to an underestimate of the cross section at high t.

Another commonly used EII cross section is the empirical formula developed by Drawin [52]. His equation has been given in several other publications [17,20,25,50], which are often cited in place of the original. Drawin's formula includes two scaling parameters, which he denotes as f_1 and f_2, and can be written as

$$\sigma(n\ell) = \frac{4\pi a_0^2 N (R/B)^2}{t}\left[f_1|s|^2\left(1 - \frac{1}{t}\right)\ln(1.25 f_2 t)\right] \tag{9}$$

Here, the reduced dipole length $|s|$ is typically set to a value of $|s|^2 = 2/3$ [52,50]. This formulation has been used by Taylor and Ali [8], Johnston [11], and Panesi et al. [12]. They all appear to have set both f_1 and f_2 equal to 1, but their papers are not clear on the subject. For the ground term, the Drawin formula overestimates the cross section at low energies. This is likely due to the lack of the binary encounter correction and the missing interference term of the Mott cross section. At higher energies, the Drawin cross section underestimates the cross section, likely because the formula approaches the Bethe limit but is missing the direct term of the Mott cross section.

Given the empirical nature of the Drawin equation, it is difficult to use the formula for higher states in which no benchmark experimental data are available. When setting $f_1|s|^2 = 2/3$ and $f_2 = 1$ in Figs. 2 and 3, the data are seen to underestimate the BEB cross section for $n \geq 3$. But given the lack of experimental data, the selected values of $f_1|s|^2$ and f_2 are somewhat subjective, and their chosen values can significantly affect the data generated. For example, Bultel et al. [53] set $f_1|s|^2 = 1$ and $f_2 = 4$ in their CR model of Earth reentry for $i \geq 4$. This model was later adapted by Panesi and Lani [33]. In Figs. 4 and 5, we compare the Drawin formula for $f_1|s|^2 = 2/3$ and $f_2 = 1$ as well as $f_1|s|^2 = 1$ and $f_2 = 4$, along with the BEB and BSR data presented earlier. It is clear that the use of $f_1|s|^2 = 1$ and $f_2 = 4$ systematically overestimates the cross section for all energies, independent of n. For their treatment of the ground and metastable states ($i = 1$–3), Bultel et al. [53] generate EII data using the same sources as Panesi et al. [12], shown in Table 1.

Lastly, Park [6] used the empirical formula of Lotz [21], who provided fitting parameters for the ground configuration. As can be seen in Fig. 2, there is reasonable agreement between the Lotz formula and the BEB and BSR results for the ground term. However, the empirical nature of the formula limits its applicability to excited states, for which experimental data are unavailable. Without these data, the ground configuration parameters must be used. Figures 2 and 3 show that these parameters do not appear suitable for higher terms, where the Lotz formula systematically underestimates the BEB.

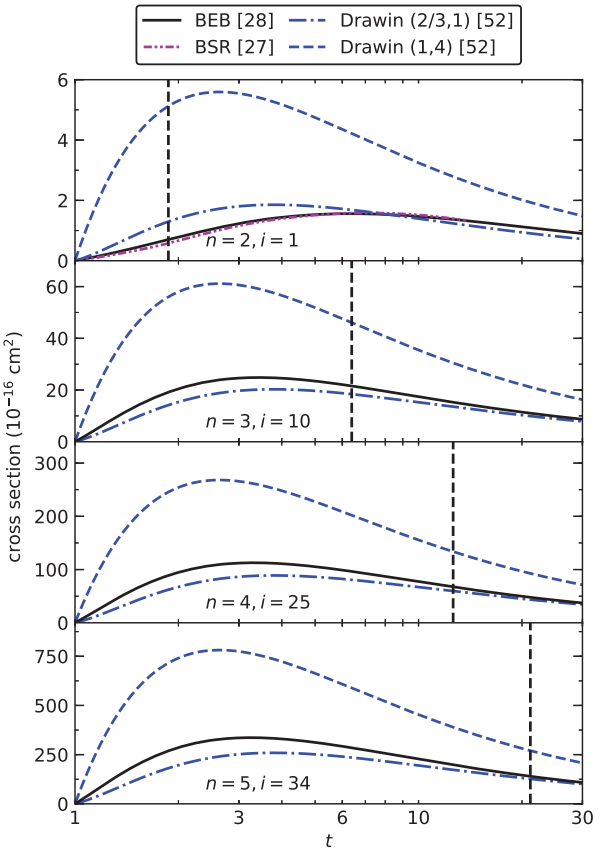

Fig. 4 Same as Fig. 2 for the BEB, BSR, and Drawin theories. See text for details.

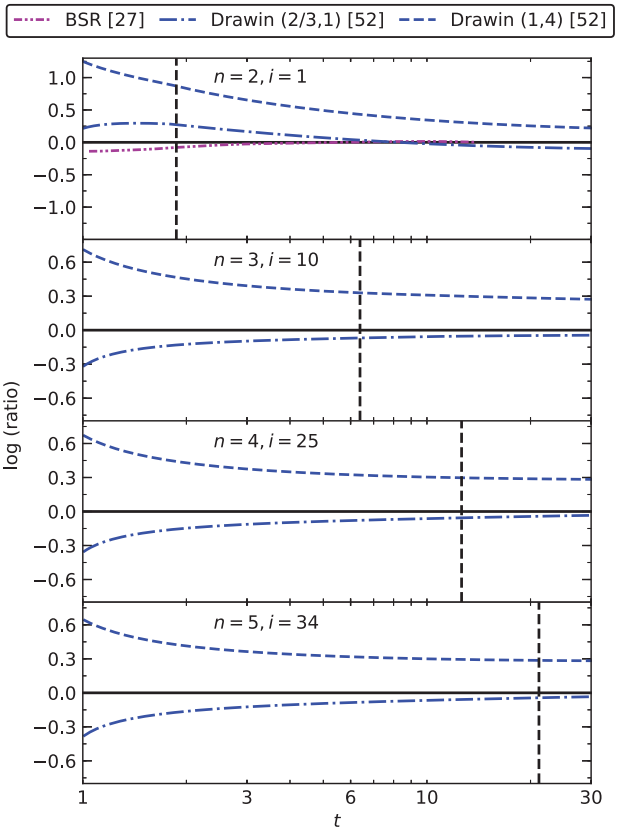

Fig. 5 Same as Fig. 3 but for the ratio of the EII cross section from the BSR and Drawin theories to that of the BEB method.

Comparing the cross-section behavior seen in Figs. 2–4, we note that there is little change in the energy dependence with n for $n \geq 3$. In part, this is because the terms in the square brackets in Eqs. (4), (5), and (7–9) depend just on the reduced translational energy. Only the magnitude of the cross section varies with n, primarily due to the binding energy term B^{-2}, which scales roughly as n^4. There is a dependence on u in the BEB and Gryziński and Kunc theories; however, for $i \geq 4$, this quantity is ≈ 1 and therefore does not significantly alter the cross-section dependence on t.

Moving now to the experimental data, a number of groups have also used the measurements of Brook et al. [16], despite the apparent metastable contamination in those data. Kunc and Soon [9] and Bourdon and Vervisch [10] both used the Brook et al. data as if it were the EII cross section for the ground term. For the two metastable terms, these groups then scaled the Brook et al. data using the procedure of Sobelman et al. [18]. Panesi et al. [12] also appear to have used the data of Brook et al., as cited by Tawara and Kato [23], for the EII cross section of ground term. For those wishing to use laboratory measurements, it would be nice to have new experimental data for ground state atomic N, free of any metastable contamination. However, the need for such measurements does not really appear to be very pressing because the BSR calculations are unlikely to be significantly in error for the ground term.

V. Rate Coefficient Calculations

Based on the preceding discussions and comparisons, for our EII model of atomic N, we have opted to use the BSR results of Wang et al. [27] for $i = 1$–3 and the BEB theory of Hwang et al. [28] for the remaining states. From these data, we have generated a thermal EII rate coefficient k_i for state i by multiplying the corresponding cross section σ_i times the relative collision velocity (essentially the electron velocity v_e) and integrating over an MB EED, $f(T, \mathcal{T}_e)$:

$$k_i(\mathcal{T}_e) = \int_{B_i}^{\infty} \sigma_i v_e f(T, \mathcal{T}_e)\, \mathrm{d}T \tag{10}$$

For hypersonic conditions, Bultel et al. [53] found that the free electrons reach an MB distribution before the atoms and molecules reach electronic and chemical equilibrium. This implies that the use of an MB EED is appropriate, regardless of other possible nonequilibrium conditions in the flowfield.

After carrying out the preceding integral, it is convenient to fit the data to a simple functional form for use in chemical models. We have fit our rate coefficient results using the Arrhenius–Kooij equation [54]:

$$k_i(\mathcal{T}_e) = \alpha_i \mathcal{T}_e^{\beta_i} \exp\left(\frac{-\gamma_i}{\mathcal{T}_e}\right) \tag{11}$$

as is commonly used in hypersonic chemistry. Here α_i, β_i, and γ_i are fitting parameters that together describe the EII rate coefficient for a given state i. The values for these parameters are presented in Table 2 for our 67-state system. We have also fit the rate coefficient data for the grouped states; these values are presented in Table 3 for use in Eq. (11) with $i = j$. For both the fine- and coarse-grain models, our rate coefficient fits match the integrated results from Eq. (10) to within $\pm 5\%$ over the temperature $T_e = 2000$–$50{,}000$ K and between 1000 and 2000 K to within $\pm 25\%$. Our EII rate coefficient data can be readily implemented into CR models. Additionally, using detailed balance, these data can be used to generate TBR rate coefficients.

VI. Conclusions

New electron-impact ionization (EII) data have been presented for a 67-state model of the electronic structure of atomic N. For the ground and metastable terms, published BSR calculations were used. For higher states, the binary-encounter dipole (BED) method was used. Though there are no benchmark measurements for EII of N for $n \geq 3$, there is a high degree of confidence in the BEB theory because it has been extensively benchmarked on other systems and includes physical processes that are not accounted for in the classical theories or the empirical fits. From these BSR and BEB data, state-specific thermal rate coefficients have been generated. Additionally, rate coefficient data have been calculated for a reduced 10-state system for use in coarse-grain simulations. Last, Arrhenius–Kooij fitting parameters have been provided for both the fine- and coarse-grain models. The present data can also be used to generate rate coefficients for three-body electron–ion recombination, the time-reverse process of EII. These new data are expected to be more accurate than those previously used. The present data will also enable modelers to move away from the quasi-steady state approximation. Taken all together, these new data will help to reduce the modeling uncertainties for the predicted radiative heating on the afterbody of a vehicle during entry into Earth's atmosphere.

Acknowledgments

This work was supported in part by the National Science Foundation (NSF) Research Experience for Undergraduates Program award PHY-1659528, by the NASA Astrophysics Research and Analysis Program grant NNX15AL73G, and by the NASA Solar System Exploration Virtual Institute Program award 80ARC017M0005. The authors thank Nigel Badnell, Klaus Bartschat, Taylor Copeland, Michael Hahn, Jose Lopez, Gillian Nave, Mitch Pindzola, Rory Vander Valk, and Oleg Zatsarinny for stimulating discussions.

References

[1] Park, C., *Nonequilibrium Hypersonic Aerothermodynamics*, 1st ed., Wiley, New York, 1990.

[2] West, T. K., IV, Johnston, C. O., and Hosder, S., "Uncertainty and Sensitivity Analysis of Afterbody Radiative Heating Predictions for Earth Entry," *Journal of Thermophysics and Heat Transfer*, Vol. 31, No. 2, 2017, pp. 294–306. doi:10.2514/1.T4948

[3] Johnston, C., and Brandis, A., "Features of Afterbody Radiative Heating for Earth Entry," *Journal of Spacecraft and Rockets*, Vol. 52, No. 1, 2015, pp. 105–119. doi:10.2514/1.A33084

[4] Kulander, J., "Departures from the Saha Equation in an Optically Thin Nitrogen Gas," *Journal of Quantitative Spectroscopy and Radiative Transfer*, Vol. 5, No. 1, 1965, pp. 253–269. doi:10.1016/0022-4073(65)90044-0

[5] Park, C., "Spectral Line Intensities in a Nonequilibrium Nitrogen Plasma," *Journal of Quantitative Spectroscopy and Radiative Transfer*, Vol. 8, No. 10, 1968, pp. 1633–1653. doi:10.1016/0022-4073(68)90107-6

[6] Park, C., "Comparison of Electron and Electronic Temperatures in Recombining Nozzle Flow of Ionized Nitrogen-Hydrogen Mixture. Part 1. Theory," *Journal of Plasma Physics*, Vol. 9, No. 2, 1973, pp. 187–215. doi:10.1017/S0022377800007431

[7] Potapov, A., Tsvetkova, L., Antropov, V., and Volkova, G., "Ionization and Radiation Characteristics of a Nonequilibrium Atomic Nitrogen Plasma," *Optical Spectroscopy*, Vol. 43, No. 3, 1977, pp. 412–417.

[8] Taylor, R., and Ali, A., "Saha Decrements and Collisional-Radiaitve Recombination and Ionization Coefficients for a Nonequilibrium Nitrogen Plasma," *Journal of Quantitative Spectroscopy and Radiative Transfer*, Vol. 35, No. 3, 1986, pp. 213–230. doi:10.1016/0022-4073(86)90046-4

[9] Kunc, J., and Soon, W., "Collisional–Radiative Nonequilibrium in Partially Ionized Atomic Nitrogen," *Physical Review A*, Vol. 40, No. 10, 1989, pp. 5822–5843. doi:10.1103/PhysRevA.40.5822

[10] Bourdon, A., and Vervisch, P., "Three-Body Recombination Rate of Atomic Nitrogen in Low-Pressure Plasma Flows," *Physical Review E*, Vol. 54, No. 2, 1996, pp. 1888–1898. doi:10.1103/PhysRevE.54.1888

[11] Johnston, C., "Nonequilibrium Shock-Layer Radiative Heating for Earth and Titan Entry," Ph.D. Thesis, Virginia Polytechnic Institute and State Univ., Blacksburg, VA, 2006.

[12] Panesi, M., Magin, T., Bourdon, A., Bultel, A., and Chazot, O., "Fire II Flight Experiment Analysis by Means of a Collisional–Radiative Model," *Journal of Thermophysics and Heat Transfer*, Vol. 23, No. 2, 2009, pp. 236–248. doi:10.2514/1.39034

[13] Annaloro, J., Morel, V., Bultel, A., and Omaly, P., "Global Rate Coefficients for Ionization and Recombination of Carbon, Nitrogen,

Oxygen and Argon," *Physics of Plasmas*, Vol. 19, No. 7, 2012, Paper 073515.
doi:10.1063/1.4737147
[14] Zipf, E., "The Ionization of Atomic Oxygen by Electron Impact," *Planetary Space Science*, Vol. 33, No. 11, 1985, pp. 1303–1307.
doi:10.1016/0032-0633(85)90008-X
[15] Thompson, W., Shah, M., and Gilbody, H., "Single and Double Ionization of Atomic Oxygen by Electron Impact," *Journal of Physics B*, Vol. 28, No. 7, 1995, pp. 1321–1330.
doi:10.1088/0953-4075/28/7/023
[16] Brook, E., Harrison, M., and Smith, A., "Measurements of the Electron Impact Ionization Cross Sections of He, C, O, and N Atoms," *Journal of Physics B*, Vol. 11, No. 17, 1978, pp. 3115–3132.
doi:10.1088/0022-3700/11/17/021
[17] Drawin, H., "Influence of Atom-Atom Collisions on the Collisional–Radiative Ionization and Recombination Coefficients of Hydrogen Plasma," *Zeitschrift für Physik A*, Vol. 225, No. 5, 1969, pp. 483–493.
doi:10.1007/BF01392775
[18] Sobelman, I., Vainshtein, L., and Yukov, E., *Excitation of Atoms and Broadening of Spectral Lines*, Springer–Verlag, New York, 1981.
[19] Gryziński, M., and Kunc, J., "Collisional Ionisation and the Atomic Model," *Journal of Physics B*, Vol. 19, No. 16, 1986, pp. 2479–2504.
doi:10.1088/0022-3700/19/16/009
[20] Drawin, H., "Collision and Transport Cross Sections," *Plasma Diagnostics*, edited by A. W. Lochte-Holtgreven, North Holland, The Netherlands, 1968, pp. 842–876.
[21] Lotz, W., "An Empirical Formula for the Electron-Impact Ioniziation Cross Section," *Zeitschrift für Physik*, Vol. 206, No. 2, 1967, pp. 205–211.
doi:10.1007/BF01325928
[22] Gryziński, M., "Classical Theory of Electronic and Ionic Inelastic Collisions," *Physical Review*, Vol. 115, No. 2, 1959, pp. 374–383.
doi:10.1103/PhysRev.115.374
[23] Tawara, H., and Kato, M., "Electron Impact Ionization Data for Atoms and Ions," NIFS-DATA-51, National Institute of Fusion Science, Tokishi, Gifu-ken, Japan, 1999.
[24] Kim, Y.-K., and Desclaux, J., "Ionization of Carbon, Nitrogen, and Oxygen by Electron Impact," *Physical Review A*, Vol. 66, No. 1, 2002, Paper 012708.
doi:10.1103/PhysRevA.66.012708
[25] Drawin, H., "Atomic Cross Sections for Inelastic Electronic Collisions," Association Euratom-CEA, Rept. EUR-CEA-FC 236, Cadarache, France, 1963.
[26] Thomson, J., "XLII. Ionization by Moving Electrified Particles," *London, Edinburgh, and Dublin Philosophical Magazine and Journal of Science*, Vol. 23, No. 136, 1912, pp. 449–457.
doi:10.1080/14786440408637241
[27] Wang, Y., Zatsarinny, O., and Bartschat, K., "*B*-Spline *R*-Matrix-with-Pseudostates Calculations for Electron-Impact Excitation and Ionization of Nitrogen," *Physical Review A*, Vol. 89, No. 6, 2014, Paper 062714.
doi:10.1103/PhysRevA.89.062714
[28] Hwang, W., Kim, Y.-K., and Rudd, M. E., "New Model for Electron-Impact Ionization Cross Sections of Molecules," *Journal of Chemical Physics*, Vol. 104, No. 8, 1996, pp. 2956–2966.
doi:10.1063/1.471116
[29] Kramida, A., Ralchenko, Y., and Reader, J., "NIST Atomic Spectra Database," National Institute of Standards and Technology, TR, Gaithersburg, MD, 2016, https://www.nist.gov/pml/atomic-spectra-database.
[30] Eriksson, K.-B., "Additions to the Spectrum of the Neutral Nitrogen Atom," *Physica Scripta*, Vol. 34, No. 3, 1986, pp. 211–215.
doi:10.1088/0031-8949/34/3/006
[31] de Beer, E., de Lange, C., and Westwood, N., "Resonance-Enhanced Multiphoton-Ionization Photoelectron Spectroscopy of np and nf Rydberg States of Atomic Nitrogen," *Physical Review A*, Vol. 46, No. 9, 1992, pp. 5653–5665.
doi:10.1103/PhysRevA.46.5653
[32] Fischer, C., Brage, T., and Jönsson, P., *Computational Atomic Structure, an MCHF Approach*, OP Publ., Bristol, England, U.K., 1997.
[33] Panesi, M., and Lani, A., "Collisional Radiative Coarse-Grain Model for Ionization in Air," *Physics of Fluids*, Vol. 25, No. 5, 2013, Paper 057101.
doi:10.1063/1.4804388
[34] Lopez, B., Johnston, C., and Panesi, M., "Improved Non-Boltzmann Modeling for Nitrogen Atoms," *46th AIAA Thermophysics Conference*, AIAA Paper 2016-4431, June 2016.
doi:10.2514/6.2016-4431
[35] Abdel-Naby, S., Pindzola, M., Pearce, A., Ballance, C., and Loch, S., "Electron-Impaction Ionization of the N Atom," *Journal of Physics B*, Vol. 48, No. 2, 2014, Paper 025203.
doi:10.1088/0953-4075/48/2/025203
[36] Krause, M., "Atomic Radiative and Radiationless Yields for K and L Shells," *Journal of Physical and Chemical Reference Data*, Vol. 8, No. 2, 1979, pp. 307–327.
doi:10.1063/1.555594
[37] Cowan, R., *The Theory of Atomic Structure and Spectra*, 1st ed., Univ. of California Press, Berkeley, CA, 1981, p. 557.
[38] Fogle, M., Bahati, E., Bannister, M., Vane, C., Loch, S., Pindzola, M., Ballance, C., Thomas, R., Zhaunerchyk, V., and Bryans, P., et al., "Electron-Impact Ionization of Be-Like C III, N IV, and O V," *Astrophysical Journal Supplemental Series*, Vol. 175, No. 2, 2008, pp. 543–556.
doi:10.1086/520852
[39] Kim, Y.-K., and Rudd, M. E., "Binary-Encounter-Dipole Model for Electron-Impact Ionization," *Physical Review A*, Vol. 50, No. 5, 1994, pp. 3954–3967.
doi:10.1103/PhysRevA.50.3954
[40] Kim, Y.-K., Inkura, K., Rudd, M., Ali, M., Stone, P., Chang, J., Coursey, J., Dragoset, R., Kishore, A., and Olsen, K., et al., "Electron-Impact Cross Sections for Ionization and Excitation Database," National Institute of Standards and Technology, Gaithersburg, MD, 2005, https://physics.nist.gov/PhysRefData/Ionization/intro.html.
[41] Huo, W., "Convergent Series Representation for the Generalized Oscillator Strength of Electron-Impact Ionization and an Improved Binary-Encounter-Dipole Method," *Physical Review A*, Vol. 64, No. 4, 2001, Paper 042719.
doi:10.1103/PhysRevA.64.042719
[42] Huo, W., and Kim, Y.-K., "Electron Collision Cross-Section Data for Plasma Modeling," *IEEE Transactions on Plasma Science*, Vol. 27, No. 5, 1999, pp. 1225–1240.
doi:10.1109/27.799798
[43] Huo, W., and Kim, Y.-K., "Use of Relativistic Effective Core Potentials in the Calculation of Total Electron-Impact Ionization Cross-Sections," *Chemical Physics Letters*, Vol. 319, No. 5, 2000, pp. 576–586.
doi:10.1016/S0009-2614(00)00150-0
[44] Kim, Y.-K., and Stone, P., "Ionization of Boron, Aluminum, Gallium, and Indium by Electron Impact," *Physical Review A*, Vol. 64, No. 5, 2001, Paper 052707.
doi:10.1103/PhysRevA.64.052707
[45] Huo, W., "Electron-Impact Excitation and Ionization in Air," von Karman Institute Lecture Series 1, RTO-EN-AVT-162, Rhode-St.-Genèse Belgium, 2009, Chap. 6.
[46] Kim, Y.-K., "Total Ionization Cross Sections of Molecules by Electron Impact," *Gaseous Dielectrics*, edited by L. C. Christophorou, J. K. Olthoff, and P. Vassiliou, Springer, New York, 2004, pp. 3–12.
[47] Ali, M. A., Irikura, K., and Kim, Y.-K., "Electron-Impact Total Ionization Cross Sections of SF_x ($x = 1$–5)," *International Journal of Mass Spectrometry*, Vol. 201, Nos. 1–3, 2000, pp. 187–195.
doi:10.1016/S1387-3806(00)00211-6
[48] Allen, C., *Astrophysical Quantities*, Athlone Press, London, 1955, p. 39.
[49] Seaton, M., "The Theory of Excitation and Ionization by Electron Impact," *Atomic and Molecular Processes*, edited by D. R. Bates, Academic Press, New York, 1962, pp. 374–420.
[50] Drawin, H., "Collision and Transport Cross Sections," Rept. EUR-CEA-FC-383, CEA-EURATOM, Groupe de Recherches sur la Fusion Fontenay-aux-Roses, France, 1967.
[51] Bely, O., and van Regemorter, H., "Excitation and Ionization by Electron Impact," *Annual Review of Astronomy and Astrophysics*, Vol. 8, No. 1, 1970, pp. 329–368.
doi:10.1146/annurev.aa.08.090170.001553
[52] Drawin, H., "Zur formelmäßigen Darstellung der Ionisierungsquerschnitte Gegenüber Elektronenstoß," *Zeitschrift für Physik*, Vol. 164, No. 5, 1961, pp. 513–521.
doi:10.1007/BF01378424
[53] Bultel, A., Chéron, B., Bourdon, A., Motapon, O., and Schneider, I., "Collisional–Radiative Model in Air for Earth Re-Entry Problems," *Physics of Plasmas*, Vol. 13, No. 4, 2006, Paper 043502.
doi:10.1063/1.2194827
[54] Lindler, K., "The Development of the Arrhenius Equation," *Journal of Chemical Education*, Vol. 61, No. 6, 1984, pp. 494–498.
doi:10.1021/ed061p494